ESTIMATION DU FLUX DE CHALEUR IMPOSÉ PAR UNE DIODE LASER SUR UNE PATE.

ESTIMATION OF THE HEAT FLUX IMPOSED BY A DIODE-LASER ON A PASTE.

Cristiano Henrique da SILVA JÚNIOR[1], Dorian BARRETTAPIANA[2], Helcio ORLANDE[1*], Modesto José LUIS DA GAMA[1]

[1]Mechanical Engineering Program, Federal University of Rio de Janeiro, COPPE/UFRJ
Cidade Universitária - Rio de Janeiro (Brazil)
[2] École Polytechnique Universitaire de Marseille
5 rue Enrico Fermi 13013 Marseille (France)
*(Corresponding author: helcio@mecanica.coppe.ufrj.br)

Résumé - Dans ce travail, le flux thermique d'une diode laser sur un échantillon d'une pate a été estimé en résolvant un problème inverse d'estimation de paramètres à partir de mesures de température réalisées avec une caméra infrarouge. Le flux du laser, modélisé par une fonction gaussienne, a été estimé par des techniques classiques et bayésiennes. Les propriétés de la pate ont été fixées ou modélisées statistiquement selon la méthode utilisée. Les résultats, comparés et analysés, s'inscrivent dans un projet de développement de matériaux pour l'impression 3D de phantoms destinés à l'étude du traitement thermique du cancer.

Abstract - In this work, the heat flux of a diode laser on a paste sample was estimated by solving an inverse parameter estimation problem using temperature measurements obtained with an infrared camera. The laser flux, modeled as a Gaussian function, was estimated using classical techniques and a Bayesian method. The paste properties were either fixed or statistically modeled depending on the method used. The results were compared and analyzed, within the scope of a project to develop materials for 3D printing of phantoms designed for studying the thermal treatment of cancer.

Nomenclature

b	sample radius, m
c	sample height, m
C	volumetric heat capacity, $\mathrm{J/m^3K}$
J	Bessel function
$\mathbf{J}$	sensitivity matrix
k	thermal conductivity, $\mathrm{W/mK}$
q	heat flux, $\mathrm{W/m^2}$
S	objective function, $\mathrm{K^2}$
t	time, s
T	temperature, K

Greek symbols

α	thermal diffusivity, $\mathrm{m^2/s}$
β	eingenvalue in r or step size
η	eingenvalue in z
σ	decay factor, m
θ	temperature variation, K

Index and exponent

0	initial or central
∞	surroundings

1. Introduction

Cancer is the second leading cause of death worldwide [1]. The scientific community has consistently devoted efforts to develop effective treatments for this disease. As a result, cancer

https://doi.org/10.25855/SFT2025-058

thermal therapies are expanding, with hyperthermia emerging as an increasingly recognized modality in the treatment of the disease.

Hyperthermia usually refers to an increase in the temperature of a region of the body to approximately 41–45° C. For cancer treatment, hyperthermia can induce tumor cell death, and is particularly effective when used in conjunction with other conventional treatments, like chemotherapy or radiotherapy [2, 3, 4]. External energy sources, such as lasers, radio frequency electrodes, or ultrasound transducers, can be used to induce hyperthermia in specific areas of the body containing a tumor [5]. Therefore, the understanding of the energy supplied by these external sources becomes an important step in the study of the hyperthermia treatment of cancer.

This work focuses on estimating the heat flux imposed by a diode-laser on the surface of a paste, which might be used to produce phantoms for hyperthermia *in-vitro* studies. Different inverse problem techniques are used to estimate parameters of a functional form assumed for the spatial distribution of the heat flux. The experimental setup is described in the next section, which is followed by a detailed description of the physical problem and its mathematical formulation. The inverse problem techniques and a discussion of the results obtained in this work are then presented. Finally, conclusions are drawn in the last section of the paper.

2. Experimental setup

The experiment consisted of heating a commercial paste (SENSODYNE toothpaste) with a diode-laser for approximately 77 seconds. The paste was carefully introduced into a container, in order to obtain a homogeneous sample of the material. The container was cylindrical with internal dimensions $b = 25$ mm of radius and $c = 20$ mm of height, made of a thermoplastic polymer (ABS GP35). Heating was promoted by a diode-laser beam, directed along the central axis of the sample and perpendicular to its top surface. The top surface of the sample was painted with a graphite ink of high absorptivity, to locally maximize the absorption of the energy of the diode-laser beam.

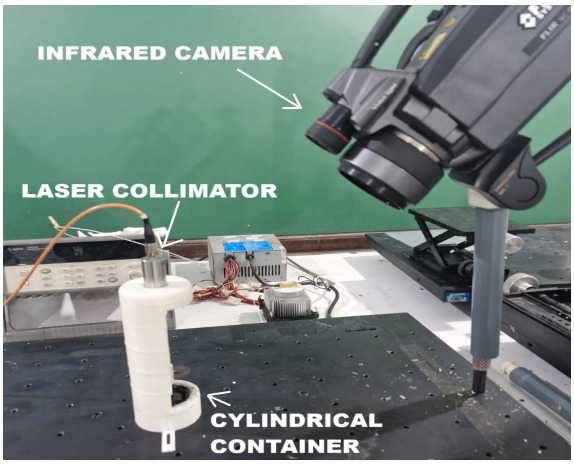

Figure 1 : *Experimental Setup*

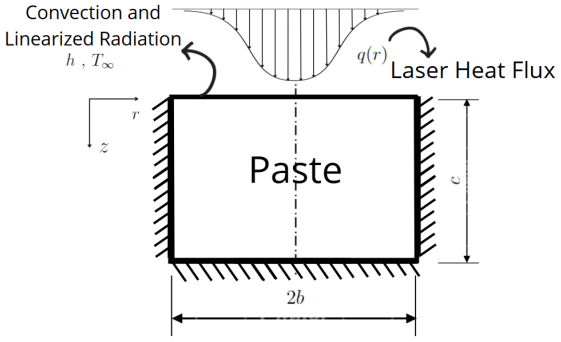

Figure 2 : *Schematic diagram of the physical problem.*

Temperature measurements on the top surface of the sample were taken with a FLIR SC660 infrared camera, with a spectral range from 7.5 to 13 μm. The camera has a resolution of 640×480 pixels and was positioned at a 45° angle relative to the vertical axis of the cylindrical sample. An emissivity of 1 was internally set in the camera software, because of the graphite ink used to paint the sample top surface. During the 76.8s of heating, 679 frames were captured

by the camera. The diode-laser setup consisted of an optical fiber connected to a NEWPORT 525B laser module, with a wavelength of 829.1 nm. A collimator (THORLABS) was used to impose the diode-laser beam to the top surface of the sample. The equipment TCi/C-Therm was used to measure the properties of the paste used in this work. This equipment is based on the Transient Plane Source method, thus providing results for thermal effusivity and thermal conductivity. The volumetric heat capacity was calculated with the values reported for these two properties. The experimental setup can be seen in Figure 1.

3. Physical problem and mathematical formulation

The physical problem addressed in this study consisted of linear transient heat conduction within the sample, in cylindrical coordinates. From analyses of previous results [4] and our own experimental data, the heat flux was assumed to vary radially as a Gaussian function, co-axial with the diode-laser beam, with no dependence on the azimuthal direction. The toothpaste was assumed to be a homogeneous and isotropic material.

For boundary conditions, it was assumed that the top surface exchanged heat with the surroundings at temperature T_∞, through convection and linearized radiation with a heat transfer coefficient h. Additionally, the diode-laser heat flux was imposed on this surface. For the lateral and bottom surfaces of the sample, it was assumed that heat exchange was negligible, as both surfaces were sufficiently distant from the diode-laser heating region. It was also considered that the sample was initially in thermal equilibrium with its surroundings at a temperature T_0. A schematic representation of the physical problem can be seen in Figure 2.

3.1. Mathematical formulation

The mathematical formulation of the above described heat conduction problem is given by:

$$\frac{1}{\alpha}\frac{\partial T(r,z,t)}{\partial t} = \frac{\partial^2 T}{\partial r^2} + \frac{1}{r}\frac{\partial T}{\partial r} + \frac{\partial^2 T}{\partial z^2}\ ,\ \ 0 \le r < b,\ \ 0 < z < c,\ \ t > 0 \tag{1}$$

$$k\frac{\partial T}{\partial r} = 0\ ,\ \ r = b,\ \ 0 < z < c,\ \ t > 0 \tag{2}$$

$$-k\frac{\partial T}{\partial z} + hT = hT_\infty + q(r)\ ,\ \ z = 0,\ \ 0 \le r < b,\ \ t > 0 \tag{3}$$

$$k\frac{\partial T}{\partial z} = 0\ ,\ \ z = c,\ \ 0 \le r < b,\ \ t > 0 \tag{4}$$

$$T(t = 0, r, z) = T_0\ ,\ \ t = 0,\ \ 0 \le r < b,\ \ 0 < z < c \tag{5}$$

The heat flux $q(r)$ was modeled as a Gaussian function with two parameters, as shown by equation (6). The parameter q_0 is the value of the diode-laser heat flux over the top surface of the sample along its axis, that is, at $r = 0, z = 0$, while σ_f is the standard deviation of the Gaussian functional form assumed for the heat flux. In order to avoid confusion with the standard deviations estimated with the solution of the inverse problem below, σ_f will be denoted henceforth as a decay factor of the Gaussian function. This work aims at the estimation of these two parameters of the heat flux function, as detailed further below.

$$q(r) = q_0 \exp\left(-\frac{1}{2}\frac{r^2}{\sigma_f^2}\right) \tag{6}$$

3.2. Solution of the direct problem

For the analytical solution of the direct problem, it was assumed that $T_0 \approx T_\infty$, and the temperature variation $\theta(r,z,t) = T(r,z,t) - T_0$ was defined. The solution was obtained with the Classical Integral Transform Technique [6] as:

$$\theta(r,z,t) = \frac{4}{b^2}\sum_{p=1}^{\infty} cos[\eta_p(c-z)]\frac{\eta_p^2+H^2}{c(\eta_p^2+H^2)+H}\widetilde{\overline{\theta}}(\beta_0=0,\eta_p,t)+ \\ + \frac{4}{b^2}\sum_{m=1}^{\infty}\sum_{p=1}^{\infty}\frac{J_0(\beta_m r)}{J_0^2(\beta_m b)}cos[\eta_p(c-z)]\frac{\eta_p^2+H^2}{c(\eta_p^2+H^2)+H}\widetilde{\overline{\theta}}(\beta_m,\eta_p,t) \quad (7)$$

where $H = h/k$. β_m and η_p are the eigenvalues given respectively by the positive roots of:

$$J_1(\beta_m b) = 0 \quad (8)$$

$$\eta_p tan(\eta_p c) = H \quad (9)$$

The integral transformed terms $\widetilde{\overline{\theta}}(\beta_0=0,\eta_p,t)$ and $\widetilde{\overline{\theta}}(\beta_m,\eta_p,t)$ are respectively written as:

$$\widetilde{\overline{\theta}}(\beta_0=0,\eta_p,t) = \frac{cos(\eta_p c)}{k\eta_p^2}\left[1-\exp\left(-\alpha\eta_p^2 t\right)\right]q_0\sigma_f^2\left(1-\exp(-b^2/2\sigma_f^2)\right) \quad (10)$$

$$\widetilde{\overline{\theta}}(\beta_m,\eta_p,t) = \frac{cos(\eta_p c)}{k(\beta_m^2+\eta_p^2)}\left[1-\exp\left(-\alpha(\beta_m^2+\eta_p^2)t\right)\right]\overline{q}(\beta_m) \quad (11)$$

In order to obtain the transformed heat flux $\overline{q}(\beta_m)$, the following integral was solved numerically using the Clenshaw-Curtis quadrature [7]:

$$\overline{q}(\beta_m) = \int_{r=0}^{b} r J_0(\beta_m r) q_0 \exp\left[\frac{-r^2}{2\sigma_f^2}\right]dr \quad (12)$$

4. Inverse problem

4.1. Basic concepts

The vector of N model parameters in the mathematical formulation of the direct problem is denoted by $\vec{P} = [P_1, P_2, ..., P_N]^T$. The transient temperature measurements at I different times, which are available for the solution of the inverse problem, are given by the vector $\vec{Y} = [Y_1, Y_2, ..., Y_I]^T$. It was assumed that the measurement errors were additive, Gaussian random variables, with zero mean and known covariance matrix $\boldsymbol{W}$. Then, the likelihood function (conditional probability density of $\vec{Y}$ with a fixed parameter vector $\vec{P}$) can be written as [8]:

$$\pi(\vec{Y}|\vec{P}) = (2\pi)^{-I/2}|\mathbf{W}|^{-1/2}\exp\left\{-\frac{1}{2}[\vec{Y}-\vec{T}(\vec{P})]^T\mathbf{W}^{-1}[\vec{Y}-\vec{T}(\vec{P})]\right\} \quad (13)$$

4.2. Classical methods

The classical techniques used in this work were based on estimating the parameters $\vec{P}$ that maximize the likelihood function, for uncorrelated measurement errors with constant variances, that is, $\boldsymbol{W} = \sigma^2\boldsymbol{I}$. Thus, the inverse problem solution can be obtained through the minimization of the least squares objective function given by[8]:

$$S_{ML} = [\vec{Y}-\vec{T}(\vec{P})]^T[\vec{Y}-\vec{T}(\vec{P})] \quad (14)$$

4.2.1. Levenberg-Marquardt method

The Levenberg-Marquardt method was devised to iteratively alleviate the ill-conditioned character of the inverse parameter estimation problem. The iterative procedure of this method is given by [8]:

$$\vec{P}^{k+1} = \vec{P}^{k} + [\mathbf{J}^T\mathbf{J} + \mu^k\mathbf{\Omega}^k]^{-1}\mathbf{J}^T[\vec{Y} - \vec{T}(\vec{P}^k)] \tag{15}$$

where $\mathbf{J}$ is the sensitivity matrix. In this work, the matrix $\mathbf{\Omega}^k$ was given by $diag[\mathbf{J}^T\mathbf{J}]$.

4.2.2. Conjugate gradient method

This method minimizes the objective function through an iterative process given by $\vec{P}^{k+1} = \vec{P}^{k} + \beta^k\vec{d}^k$, where $\vec{d}^k$ is the direction of descent and β^k is the step size at iteration k. The following expression for β^k is obtained by a linearization procedure and the minimization of the objective function along the given direction of descent [8]:

$$\beta^k = \frac{[\mathbf{J}^k\vec{d}^k]^T[\vec{Y} - \vec{T}(\vec{P}^k)]}{[\mathbf{J}^k\vec{d}^k]^T[\mathbf{J}^k\vec{d}^k]} \tag{16}$$

The direction of descent involves a linear combination of the negative gradient direction and the direction of descent from the previous iteration, that is,

$$\vec{d}^k = -\nabla S_{ML}(\vec{P}^k) + \gamma^k\vec{d}^{k-1} \tag{17}$$

Two versions of the method were used for calculating the conjugation coefficient γ^k. In the Fletcher-Reeves version, we have:

$$\gamma^k = \frac{[\nabla S_{ML}(\vec{P}^k)]^T[\nabla S_{ML}(\vec{P}^k)]}{[\nabla S_{ML}(\vec{P}^{k-1})]^T[\nabla S_{ML}(\vec{P}^{k-1})]}\,, \text{ with } \gamma^0 = 0 \text{ for } k = 0 \tag{18}$$

while for the Polak-Ribiere version we have:

$$\gamma^k = \frac{[\nabla S_{ML}(\vec{P}^k)]^T[\nabla S_{ML}(\vec{P}^k) - \nabla S_{ML}(\vec{P}^{k-1})]}{[\nabla S_{ML}(\vec{P}^{k-1})]^T[\nabla S_{ML}(\vec{P}^{k-1})]}\,, \text{ with } \gamma^0 = 0 \text{ for } k = 0 \tag{19}$$

Morozov's discrepancy principle was used as the stopping criterion for the iterative procedures of the Levenberg-Marquardt method and of the Conjugate Gradient method presented above.

4.3. Bayesian methods

Methods within the Bayesian framework of statistics incorporate previous information about the parameters in terms of a statistical model, $\pi(\vec{P})$. The inverse problem solution is then obtained from inference on the posterior distribution, which is the conditional probability distribution of the unknown parameters given the measurements, that is, $\pi(\vec{P}|\vec{Y})$. The posterior distribution is related to the prior distribution and to the likelihood through Bayes' theorem:

$$\pi(\vec{P}|\vec{Y}) \propto \pi(\vec{Y}|\vec{P})\pi(\vec{P}) \tag{20}$$

Markov Chain Monte Carlo methods (MCMC) are based on the generation of samples of the posterior distribution through stochastic simulations. In this work, Markov Chains were simulated using the Metropolis-Hastings algorithm [8], where a candidate for the posterior distribution is proposed with an auxiliary distribution with a certain probability of acceptance. In this work, the proposal distributions were Gaussian random-walk processes [4, 8].

5. Results and discussions

5.1. Measurements of temperatures and thermophysical properties

The infrared camera images with the temperature measurements were pre-processed with a uniform filter to reduce noise, before the solution of the inverse problem. The temperature measurements supported the hypothesis made for the boundary condition at the lateral surface of the sample, as well as for the axial symmetry of the problem. The radial temperatures were considered as the mean values obtained with pixels equidistant from the center line, at two orthogonal lines in the infrared images. Uncertainties were appropriately propagated, by considering the standard deviation of the original measurements as that obtained from the images of the sample before the heating, that is, $\sigma = 0.03$°C. The mean temperature value of these images also provided the initial condition for the problem, as $T_0 = 24.55$°C. The measurements used for the inverse problem were taken at the central point of the heated surface of the sample.

Before the experiments, the thermophysical properties of the paste were measured with the equipment TCi/C-Therm. Table 1 presents the means and standard deviations obtained with 20 measurements for thermal conductivity and volumetric heat capacity of the paste.

	k	C
	W.m^{-1}K^{-1}	kJ.m^{-3}K^{-1}
Mean	1.0455	1783.21
Std. deviation	0.0076	6.06

Table 1 : *Mean and standard deviation of the thermophysical properties*

5.2. Estimated parameters

The sensitivity coefficients of the temperature at the measurement location with respect to the model parameters were examined before the solution of the inverse problem. The sensitivity coefficients are not presented here for the sake of brevity. In summary, the sensitivity coefficient with respect to h remained with low magnitude throughout the experiment. During the first 40 s of the experiment, linear dependency was observed between the sensitivity coefficients of q_0 and C. After this time, the sensitivity coefficients with respect to σ_f and k were also linearly dependent. The sensitivity coefficients with respect to q_0 and k were linearly dependent during the whole duration of the experiment.

As a result of the analysis of the sensitivity coefficients, for the classical methods the thermophysical properties k and C were deterministically set with the mean values presented in Table 1. The value of h was also fixed as 10 W.m^{-2}.K^{-1}, corresponding to the natural convection and linearized radiation heat transfer conditions during the experiment. The parameters were estimated with initial estimates of 8.5 mm for the decay factor and 440.57 W.m^{-2} for the central heat flux, in the iterative procedures of the classical methods, as well as for the Metropolis-Hastings algorithm. Table 2 shows the results obtained with the classical methods considered here. The Levenberg-Marquardt method provided the best estimate, yielding the smallest value of the objective function with uncorrelated residuals, and also requiring the smallest number of iterations. Both versions of the conjugate gradient method required more iterations to reach Morozov's criteria and also exhibited residuals more correlated, than those obtained with the Levenberg-Marquardt method.

	q_0	σ_f	S_{ML}	$Iterations$
	W.m^{-2}	mm	K^2	-
Levenberg-M.	375.84 $\pm$ 8.14	8.184 $\pm$ 0.578	0.0651	2
Fletcher-Reeves	376.96 $\pm$ 8.31	7.948 $\pm$ 0.552	0.1164	10
Polak-Ribiere	402.27 $\pm$ 9.31	6.728 $\pm$ 0.411	0.1288	13

Table 2 : *Classical methods estimates at 99% confidence levels*

The priors for the MCMC method were selected for the thermophysical properties as Gaussian distributions, with means and standard deviations given by their independent measurements (see Table 1). For the parameters with least informative prior information, q_0, σ_f and h, uniform distributions were modeled with lower and upper bounds of [200;800] W.m^{-2}, [2;12] mm, and [5;15] W.m^{-2}.K^{-1}, respectively. The Gaussian random-walk proposal distributions were considered with a standard deviation of 0.65% of the initial estimation for q_0 and of 0.5% for σ_f, 0.1% for k and C, and 1% for h. $30,000$ states were calculated with the Markov chains, resulting in an acceptance rate of 21.60%. The burn-in period was considered to be the first $5,000$ states. The resulting chains and histograms for the laser parameters are presented in figures 3-6. For a 99% credible level, parameters estimated with MCMC were $q_0 = 416.12 \pm 14.89$ W.m^{-2} and $\sigma_f = 7.276 \pm 0.994$ mm. Thus, although not statistically identical, the parameters estimated with the classical methods and with MCMC were not too different. Parameters estimated with the MCMC method resulted in small and uncorrelated residuals, as illustrated in Figure 7. However, for the radial temperature distribution, the model did not adequately represent the data (see Figure 8).

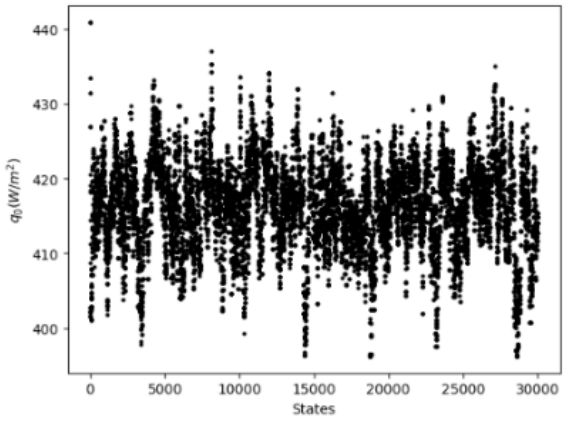

Figure 3 : *Markov chain for q_0*

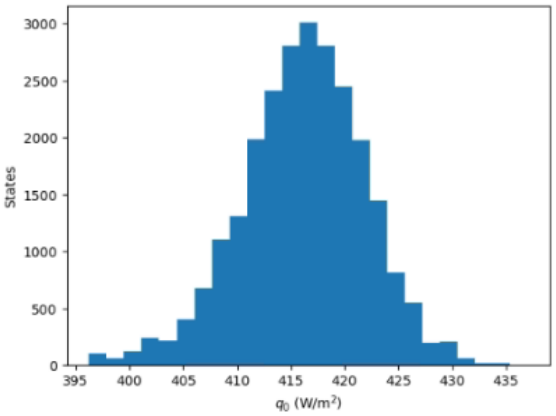

Figure 4 : *Histogram for q_0 after burn-in*

6. Conclusion

Parameters of a Gaussian functional form assumed for a heat flux imposed by a diode-laser were estimated in this work. The smallest residuals were obtained with the MCMC method, which also accounted for uncertainties in other model parameters assumed as deterministically known for the classical methods. Ongoing work currently involves the use of function estimation techniques within the Bayesian framework of statistics, to improve the agreement between measured and estimated temperatures at other radial positions.

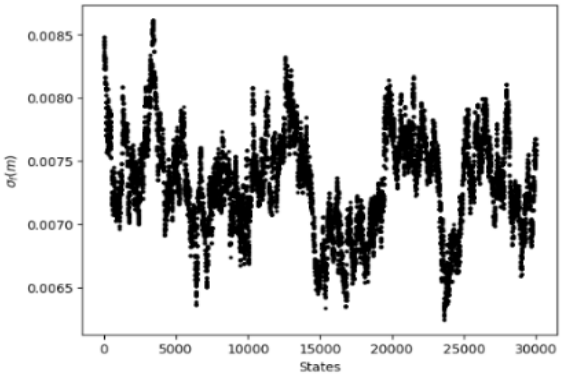

Figure 5 : *Markov chain for* σ_f

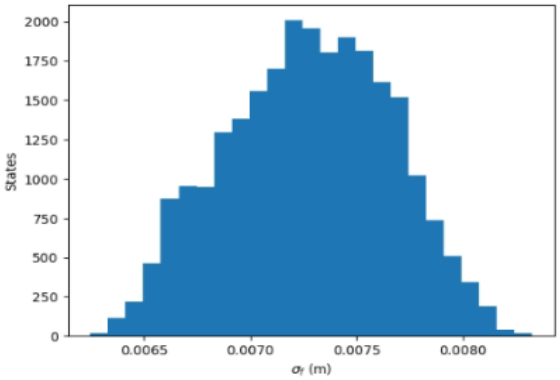

Figure 6 : *Histogram for* σ_f *after burn-in*

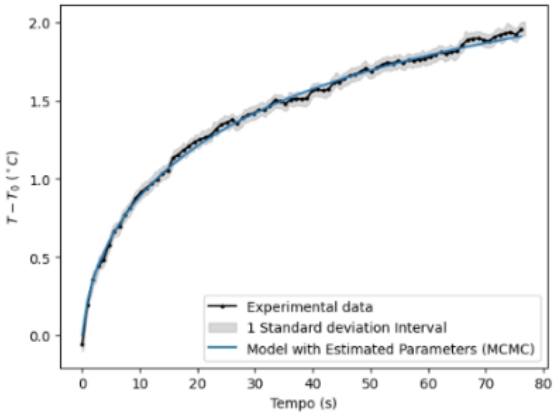

Figure 7 : *MCMC estimate at* $(r = 0, z = 0)$

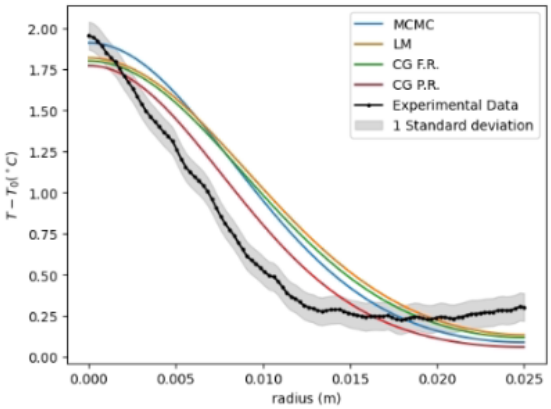

Figure 8 : *Radial distribution at* t *=76.1 s*

References

[1] D. L. Kasper, S. L. Hauser,J. L. Jameson, A. S. Fauci, D. L. Longo, J.h Loscalzo, *Harrison's Principles of Internal Medicine*, AMGH Editora Ltda (2017).

[2] R. W. Y. Habash, R. Bansal, D. Krewski, H. T. Alhafid, Thermal Therapy, Part 2: Hyperthermia Techniques, *Crit. Rev. in Biomed. Eng.*, (2006).

[3] B. Hildebrandt, P. Wust, O. Ahlers, A. Dieing, G. Sreenivasa, T. Kerner, R. Felix, H. Riess, The cellular and molecular basis of hyperthermia, *Crit. Rev. in Oncology/Hematology*, (2001).

[4] N. P. da Silva, L. A. B. Varon, J. M. J. da Costa, H. R. B. Orlande, Monte Carlo parameter estimation and direct simulation of in vitro hyperthermia-chemotherapy experiment, *Num. Heat Transf., Part A: Applications*, (2021).

[5] P. Cherukuri and E. S. Glazer and S. A. Curley, Targeted hyperthermia using metal nanoparticles, *Adv. Dr. Deliv. Rev.*, (2009).

[6] M. N. Ozisik, *Heat Conduction*, Wiley Interscience, (1993).

[7] C.W. Clenshaw, A.R. Curtis, A method for numerical integration on an automatic computer, *Numer. Math.*, (1960)

[8] M. N. Ozisik, H. R. B. Orlande, *Inverse Heat Transfer Fundamentals and Applications*, RC Press/Taylor & Francis, (2021).

Acknowledgements

The authors would like to acknowledge the support provided by CNPq, CAPES and FAPERJ.